**ACR Open Rheumatology**
Vol. 4, No. 4, April 2022, pp 288–299
DOI 10.1002/acr2.11384


American College of Rheumatology
Empowering Rheumatology Professionals

# Caspase-8 Variant G Regulates Rheumatoid Arthritis Fibroblast-Like Synoviocyte Aggressive Behavior

Cecilia Ansalone,[1] Richard I. Ainsworth,[1] Gyrid Nygaard,[1] Rizi Ai,[1] Edward B. Prideaux,[1] Deepa Hammaker,[1] Narayanan B. Perumal,[2] Ken Weichert,[2] Frances Tung,[2] Lalitha Kodandapani,[2] J. Michael Sauder,[2] Elisabeth C. Mertsching,[2] Robert J. Benschop,[3] David L. Boyle,[1] Wei Wang,[1] and Gary S. Firestein[1]

**Objective.** Fibroblast-like synoviocytes (FLS) play a pivotal role in rheumatoid arthritis (RA) by contributing to synovial inflammation and progressive joint damage. An imprinted epigenetic state is associated with the FLS aggressive phenotype. We identified *CASP8* (encoding for caspase-8) as a differentially marked gene and evaluated its pathogenic role in RA FLSs.

**Methods.** RA FLS lines were obtained from synovial tissues at arthroplasty and used at passage 5-8. Caspase-8 was silenced using small interfering RNA, and its effect was determined in cell adhesion, migration and invasion assays. Quantitative reverse transcription PCR and western blot were used to assess gene and protein expression, respectively. A caspase-8 selective inhibitor was used determine the role of enzymatic activity on FLS migration and invasion. Caspase-8 isoform transcripts and epigenetic marks in FLSs were analyzed in FLS public databases. Crystal structures of caspase-8B and G were determined.

**Results.** Caspase-8 deficiency in RA FLSs reduced cell adhesion, migration, and invasion independent of its catalytic activity. Epigenetic and transcriptomic analyses of RA FLSs revealed that a specific caspase-8 isoform, variant G, is the dominant isoform expressed (~80% of total caspase-8) and induced by PDGF. The crystal structures of caspase-8 variant G and B were identical except for a unique unstructured 59 amino acid N-terminal domain in variant G. Selective knockdown of caspase-8G was solely responsible for the effects of caspase-8 on calpain activity and cell invasion in FLS.

**Conclusion.** Blocking caspase-8 variant G could decrease cell invasion in diseases like RA without the potential deleterious effects of nonspecific caspase-8 inhibition.

## INTRODUCTION

Rheumatoid arthritis (RA) is an immune-mediated disease characterized by synovial inflammation and progressive joint destruction (1,2). Recent targeted therapies have markedly improved clinical outcomes, although a significant percentage of patients with RA still experience persistent inflammation and disability (3). In addition to systemic immune dysfunction, fibroblast-like synoviocytes (FLS) in the RA synovial intimal lining play a crucial role in synovitis and joint damage; they not only react to the inflammatory milieu but also display an aggressive phenotype with impaired contact inhibition, reduced apoptosis, reprogrammed cellular metabolism, and increased invasive potential (4). An imprinted epigenetic pattern in RA FLSs likely contributes to this abnormal phenotype (4,5).

Our recent epigenetic analysis integrated diverse multiplexed RA FLS epigenomic data; pathway analysis of differentially modified epigenomic regions identified common abnormalities in RA, including inflammation, immune responses, and cell migration. Unexpectedly additional novel pathways, including the

This project was supported by a grant from Eli Lilly and Company (to GSF) and a grant from the National Institute for Arthritis and Musculoskeletal and Skin Diseases (R01 AR065466 [to GSF and WW]).

[1]Cecilia Ansalone, PhD, Richard I. Ainsworth, PhD, Gyrid Nygaard, PhD, Rizi Ai, PhD, Edward B. Prideaux, MS, Deepa Hammaker, PhD, David L. Boyle, BA, Wei Wang, PhD, Gary S. Firestein, MD: University of California San Diego, La Jolla, California; [2]Narayanan B. Perumal, PhD, Ken Weichert, BS, Frances Tung, BS, Lalitha Kodandapani, PhD, J. Michael Sauder, PhD, Elisabeth C. Mertsching, PhD: Lilly Biotechnology Center, San Diego, California; [3]Robert J. Benschop, PhD: Eli Lilly and Company, Indianapolis, Indiana.

Narayanan B. Perumal, Ken Weichert, Frances Tung, Lalitha Kodandapani, J. Michael Sauder, Elisabeth C. Mertsching, and Robert J. Benschop are employees of Eli Lilly and Company. No other disclosures relevant to this article were reported.

Data availability: Protein coordinates and structure factors have been deposited in the Protein Data Bank under the access codes 7LVJ (isoform G) and 7LVM (isoform B).

Address correspondence to Gary S. Firestein, MD, and Wei Wang, MD, University of California San Diego, 9500 Gilman Drive, La Jolla, CA 92093. Email: gfirestein@health.ucsd.edu (G.S.F.); wei-wang@ucsd.edu (W. W.).

Submitted for publication May 26, 2021; accepted in revised form October 13, 2021.

"Huntington disease signaling," emerged from the analysis as unique to RA FLS (6). Biologic validation of the integrated analysis initially focused on a key structural protein, Huntingtin Interacting Protein-1 (HIP-1) (6,7). We also noted that caspase-8 is downstream of HIP-1 in the Huntington disease pathway and was identified as an abnormally marked gene in RA (8). Caspase-8 is unique among the caspases because it has non-proteolytic functions that alter cell behavior in cancer (9,10) through interactions with the focal adhesion machinery (11–14). These intriguing findings led us to explore the role of caspase-8 gene (*CASP8*) in RA.

We now report that caspase-8 regulates the invasive behavior of primary RA FLSs. Caspase-8 expression is downstream of Platelet-derived growth factor (PDGF) signaling and modulates calpain activity and talin cleavage. A detailed analysis of caspase-8 structure and function in FLSs showed that the caspase-8 transcript variant G is epigenetically abnormal in RA FLSs and is the key isoform induced by PDGF. More importantly, the G variant is responsible for regulating FLS migration and invasion independent of catalytic activity. These data demonstrate how integrating multiple omics data can identify pathogenic pathways and identify potential therapeutic targets.

## MATERIALS AND METHODS

**Fibroblast-like synoviocytes.** Tissue samples were obtained from patients with RA and patients with osteoarthritis (OA) at the time of knee or hip replacement surgery. Patients were diagnosed with RA following the American College of Rheumatology 1987 revised criteria or the 2010 criteria (15,16), and all had severe disease requiring arthroplasty. Human specimens were de-identified, and specific clinical information related to disease severity was not available. The Human Research Protection Program approved the procedure, and all patients provided written informed consent. FLSs were isolated from synovial tissues as previously described (17) and used from passage 5 through 8. Primary FLSs were cultured at 6% $CO_2$, 37°C in Gibco Dulbecco's Modified Eagle Medium (DMEM) supplemented with L-glutamine, gentamicin, penicillin/streptomycin (complete DMEM), and 10% heat-inactivated Fetal Bovine Serum (FBS) (18). Twenty different RA FLS lines were used for these experiments.

**Gene silencing.** Total caspase-8 gene silencing was performed using small interfering Smart Pool On-Target RNA (siRNA) (Dharmacon, Horizon) transfected into FLSs using the normal human dermal fibroblast Nucleofector kit, according to the manufacturer's instructions (Amaxa, Lonza). Scramble Smart Pool non-targeting siRNA was used as control. Dicer-substrate siRNA specifically targeting the N-term domain of caspase-8G were custom designed using the IDT platform (Integrated DNA Technologies; +strand: rGrCrUrGrArArUrUrUrGrCrUrArGrUrCrArArCrUrCrArACA; −strand: rUrGrUrUrGrArGrUrUrGrArCrUrArGrCrArArArUrUrCrArGrCrArG). RA FLSs were cultured at 80% confluency before being used for transfection. A total of $5 \times 10^5$ FLSs (passages 5-7) were transfected with 1 μg siRNA.

**Quantitative real-time PCR.** FLSs were lysed in RLT buffer (Qiagen) containing 1% beta-mercaptoethanol. Messanger RNA (mRNA) was extracted and purified on RNeasy mini- or micro-columns with on-column DNase digestion, according to the manufacturer's instructions (Qiagen). RNA was quantified using a NanoDrop (Thermo Fisher Scientific) and converted in complementary DNA using TaqMan reverse transcription reagents (Thermo Fisher Scientific) and a StepOne™ Real-Time PCR System (Thermo Fisher Scientific). Quantitative reverse transcription PCR (RT-qPCR) was performed using primer probes with FAM (5′), MGB Quencher (3′) from TaqMan Gene Expression Assays (Applied Biosystem, Thermo Fisher Scientific). Primer probes used for caspase-8 transcript variant analysis are listed in Table S1. TaqMan glyceraldehyde 3-phosphate dehydrogenase (GAPDH) Control Reagents with JOE (5′), TAMRA Quencher (3′) were used as control (Thermo Fisher Scientific). Relative gene expression and fold change was calculated using the comparative $C_T$ method, as previously described (19).

**Western blot.** Protein lysates were obtained, and proteins were denatured in NuPAGE™ LDS loading buffer and 100 mM dithiothreitol and fractioned on NuPAGE™ 4%-12% Bis-Tris Gels (Invitrogen, Thermo Fisher Scientific). Concentration of proteins was calculated using the Micro BCA™ Protein Assay Kit (Thermo Fisher Scientific), and equal amounts of proteins (15-30 μg) were loaded. Following blotting to polyvinylidene fluoride membranes and blocking with 5% dry milk, blots were probed with antibodies against HIP-1 (clone EPR10814; Abcam), caspase-8 (clone 1C12), or talin/FERM domain (clone TA205; BioRad). Anti-actin-β antibody (clone AC-15; Millipore Sigma) was used as loading control. Horseradish peroxidase–conjugated goat anti-rabbit or anti-mouse immunoglobulin G (Cell Signaling Technology) were used as secondary antibody. Blots were developed using an Immun-Star WesternC ECL substrate (BioRad), imaged on a VersaDoc imaging system (BioRad), and densitometry analyzed with QuantityOne software (Biorad). In certain experiments, RA FLSs were serum starved in 0.1% FBS media for 24 hours prior to stimulation with 10 ng/ml PDGF for 15, 30, and 60 minutes.

**Adhesion assay.** Ninety-six-well plates were coated overnight with either 4 $\mu g/cm^2$ fibronectin (Corning) dissolved in Hanks' Balanced Salt Solution buffer (no $Ca^{2+}$, no $Mg^{2+}$) or 10 $\mu g/cm^2$ collagen type II (Corning) in 0.05 N acetic acid. After extensive wash with Dulbecco's phosphate-buffered saline (DPBS; no $Ca^{2+}$, no $Mg^{2+}$), cells were de-attached using Accutase (BioLegend) and plated at $1 \times 10^4$ cells/well and left to adhere for 30 minutes. Nonadhered cells were removed by washing with DPBS; unwashed wells represented 100% of adhesion.

Cells were then fixed with 4% paraformaldehyde and stained with 0.2% crystal violet in 2% ethanol for 5 minutes. After extensive washing, plates were left to air dry. Crystal violet stain was dissolved with 1% sodium dodecyl sulfate and absorbance read at 550 nM. The percentage of cells that had adhered was calculated by ratio of absorbance of washed wells to unwashed wells.

**Matrigel invasion assays.** In Matrigel spheroid assay the ability of cells to evade from a 3D Matrigel micro-mass was evaluated, as previously described (20). Briefly, RA FLSs were resuspended at $2 \times 10^4$ cells/μl and mixed with one volume of Growth Factor Reduced Corning Matrigel Basement Membrane Matrix (Corning); 4 μl drop of the mixture was spotted onto a plate and left to set 5 minutes at 37°C. Warm media (complete DMEM + 10% FBS) was added and cells stimulated with PDGF-BB (10 ng/ml; Peprotech). After 24 hours, cells were fixed and stained with the Hemacolor staining kit (Millipore-Sigma) and digital images acquired. The area covered by invading cells was calculated using ImageJ software.

For the invasion migration assay, $15 \times 10^4$ cells were resuspended in serum starving media (0.1% FBS in complete DMEM), seeded into the upper chamber of Matrigel-coated invasion chambers (pore size 8.0 μm; Corning) and left to invade the below chamber in response to chemoattractant-rich media (complete DMEM + 10% FBS) in presence or not of PDGF-BB (10 ng/ml). After 24-hour incubation, cells were fixed in 100% methanol and stained with 0.2% crystal violet in 2% EtOH. Images at 4X magnification were acquired, and the invaded area was quantified with ImageJ software. PDGF-induced migration was calculated by normalization over medium alone. In some experiments, FLSs were pre-incubated with Z-IETD-fluoromethyl ketone (FMK) (Selleckchem) or vehicle control (0.01% dimethyl sulfoxide (DMSO)) for 1 hour followed by addition of PDGF-BB.

**Scratch and wound healing assay.** FLSs were cultured to 80% confluency before a linear cross wound was created using a 1 ml micropipette tip as previously described (21). Light microscopy 4X images were taken at four locations around the cross wound to determine the width at time 0. Cells were incubated with PDGF-BB (10 ng/ml) for 24 hours and then fixed and stained using a Hemacolor staining kit, following the manufacturer's instructions (Millipore-Sigma). Light microscopy 4X images for two locations of marked wound were obtained. The number of migrated cells into the wound area was quantified using ImageJ software. In some experiments, FLSs were pre-incubated with Z-IETD-FMK, Tofacitinib (CP-690550) (Selleckchem), or vehicle control (0.01% DMSO) for 1 hour prior to PDGF-BB stimulation.

**Calpain activity assay.** After 24 hours from transfection, FLSs were seeded onto 96-well plates ($10^4$ cells/well) and allowed to attach 23 hours in slow growth media (complete DMEM + 1% FBS). Media were then replaced with reaction buffer (115 mM NaCl, 1 mM $KH_2PO_4$, 5 mM KCl, 2 mM $CaCl_2$, 1.2 mM $MgSO_4$, and 25 mM HEPES [pH 7.25]), and cells were pre-incubated 1 hour with 50 μM PD150606 (a specific cell-permeable calpain-2 inhibitor; Millipore-Sigma) followed by the addition of 50 μM SLLVY-AMC (Millipore-Sigma), a cell-permeable calpain fluorescent substrate, alongside or not 10 ng/ml PGDF-BB (Peprotech). Fluorescence (355/460 nm) was recorded at different time points (0-8 h). Fold changes were calculated as relative fluorescence units (RFU) = $RFU_{SLLVY\text{-}AMC}$ /$RFU_{SLLVY\text{-}AMC+\ PD150606}$ and signal normalized on time 0.

**Chromatin immunoprecipitation and RNA sequencing analysis.** Libraries were pooled and sequenced with an Illumina HiSeq2000. Chromatin immunoprecipitation sequencing (ChIP-seq) data generation, processing, and identification of differentially modified epigenetic regions (DMERs) as well as RNA sequencing (RNA-seq) analysis data generation was performed as previously described (6). Raw read quality was evaluated using FastQC. Pair-ended raw reads were trimmed of adapters and bases with Phred scores below 15. Post-trimming reads of less than 30 bp were removed. Genome indices were generated using STAR (version 2.7.0) (22) and subsequently aligned to the human reference genome hg19. Quantification of gene and isoform expression was performed using RSEM (version 1.3.1) (23). The data used in this study are available in Gene Expression Omnibus with the primary accession code GSE112658 (6).

**Caspase-8 splicing variants and conservation analysis.** DMER coordinates were mapped onto the UCSC Genome Browser (GRCh37/hg19 assembly) (24,25) with National Center for Biotechnology Information (NCBI) RefSeq genes, curated subset (Annotation Release 105.20190906 [2019-10-24]) for *CASP8* gene (26). Characterized protein-coding sequences of caspase-8 isoforms were download from the NCBI, and multiple sequence analysis was done with the EMBL-EBI Clustal Omega online software (www.ebi.ac.uk/Tools/msa/clustalo/) (27). For the conservation analysis of the N-term domain of caspase-8G, the first 60 aminoacidic sequence was run onto the online Basic Local Alignment Search Tool web interface provided by the NCBI. The top hits with Max Score ≥ 40 were further aligned using Clustal Omega (27). A taxonomy tree was created using the NCBI taxonomy database (www.ncbi.nlm.nih.gov/taxonomy) (28), and a phylogenetic tree was created using the Phylo.io online platform (29).

**Protein production and crystallography of caspase-8 death effector domain.** Experimental procedures and analysis are provided in the online Supplementary file.

**Statistical analysis.** Prism 8 (Graphpad) was used to perform all statistical analysis, and statistical tests used are indicated

in the figure legends. *P* values less than or equal to 0.05 were considered significant.

## RESULTS

**Caspase-8 and HIP-1 regulate PDGF-induced invasion in RA FLSs.** We initially evaluated potential interactions between caspase-8 and HIP-1 as regulators of FLS invasion due to their relationship in the Huntington disease pathway. Caspase-8 (all isoforms) and/or HIP-1 expression were silenced using siRNA, and the cells were assessed for PDGF-induced invasion. Forty-eight hours after transfection, transcript levels of HIP-1 and caspase-8 were reduced by 92.5% ± 1.6% and 75.4% ± 4.1%, respectively (Figure 1A). Decreased transcripts resulted in more than 60% decrease in protein levels at 72 hours post transfection (Figure 1B). HIP-1 or caspase-8 deficiency significantly reduced PDGF-induced invasion; however, combined silencing was not additive (Figure 1C and 1D). The data suggest that HIP-1 and caspase-8 are downstream of PDGF, in series rather than in parallel, and can regulate FLS invasion.

**Caspase-8 regulates FLS migration and adhesion via calpain and talin.** Caspase-8 localizes at focal adhesions in cancer cells and enhances migration and adhesion through calpain activation (11,12). Adhesion to the extracellular matrix proteins fibronectin and collagen type II and migration from Matrigel

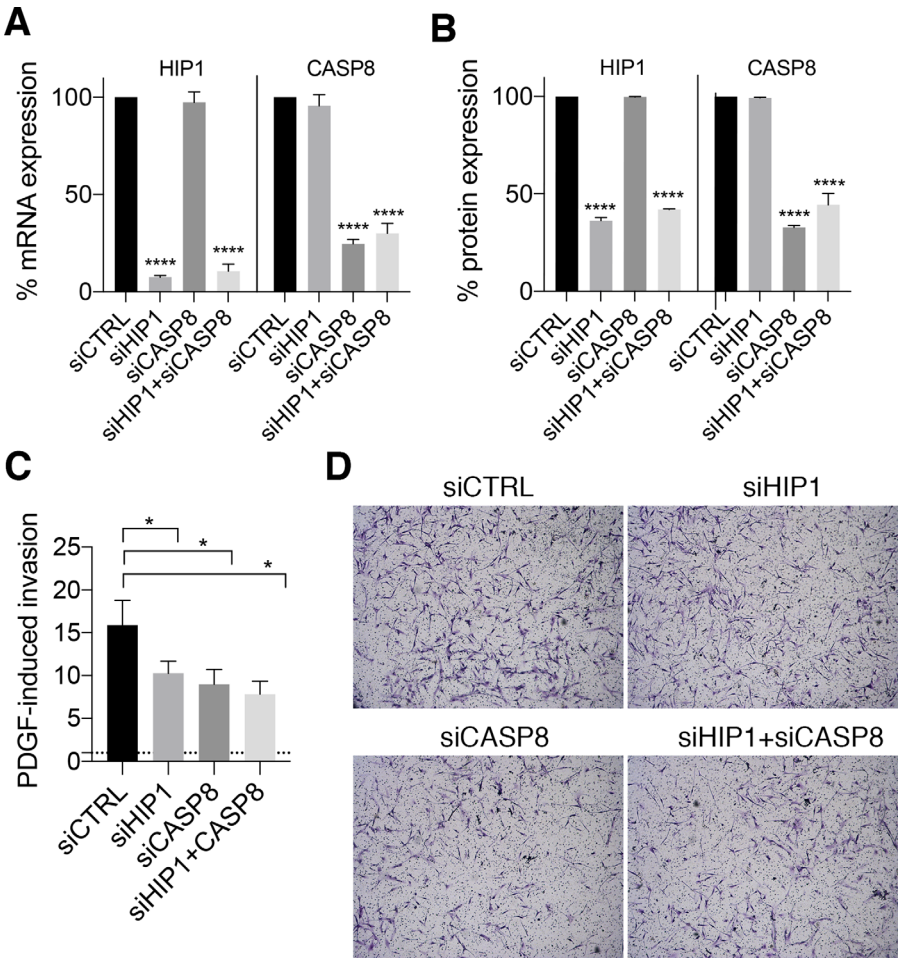


**Figure 1.** Caspase-8 and HIP-1 are part of the same pathway downstream PDGF-induced invasion in RA FLSs. FLSs were transfected with siRNA targeting caspase-8 (siCASP8), HIP-1 (siHIP-1), double-silenced siHIP-1 + siCASP8, or un-targeting control (siCTRL). Silencing efficiency on (**A**) transcript level and (**B**) protein level of HIP-1 and caspase-8 at 48 hours and 72 hours post transfection, respectively. mRNA expression was normalized to GAPDH and protein levels to actin-β. Error bars are mean ± SEM of n = 3 independent experiments. Data were analyzed with one-way ANOVA and Dunnet's multiple comparisons test, comparing to siCTRL. ****$P \leq 0.0001$. (**C**) Quantification of PDGF-induced invasion (calculated as fold change of %invaded area under PDGF divided %invaded area in media alone) and (**D**) representative 4X images of crystal violet-stained cells that had transmigrated through the Matrigel membrane after 24-hour PDGF. Time zero corresponded to 48 hours post transfection. Error bars are mean ± SEM of n = 6. Data were analyzed with one-way ANOVA and Holm-Sidak's multiple comparisons test, comparing to siCTRL. *$P \leq 0.05$. FLS, fibroblast-like synoviocyte; HIP-1, Huntingtin Interacting Protein-1; GAPDH, glyceraldehyde 3-phosphate dehydrogenase; PDGF, platelet-derived growth factor; RA, rheumatoid arthritis; siRNA, small interfering RNA.

micro-masses in caspase-8-deficient FLSs were reduced (Figure 2A and 2B). We then found that caspase-8 deficiency significantly reduced calpain activity of RA FLSs under spontaneous conditions (Figure 2C; left side). This activity was further induced by PDGF, and caspase-8 deficiency reduced it (Figure 2C; right side).

In resting cells, the talin head domain stabilizes integrin heterodimer conformation by binding to its cytosolic domain. When talin is cleaved by calpain, the FERM domain is released (13,30). PDGF increased talin cleavage in FLSs in a time-dependent fashion (Figure 2D). The effect was reduced in caspase-8-deficient cells (Figure 2E and 2F). Interestingly, silencing HIP-1 also reduced PDGF-induced calpain activity but had no effect under basal conditions (Figure S1). This aligns with the upstream role of HIP-1 on PDGF receptor β recycling and signaling (7) and suggests that caspase-8 plays a downstream role at the focal adhesions.

**Caspase-8 role in migration and invasion in RA FLSs is independent of its enzymatic activity.** The caspase-8 catalytic subunit, but not its enzymatic activity, is required for activation of the calpain–calpastatin proteolytic system and

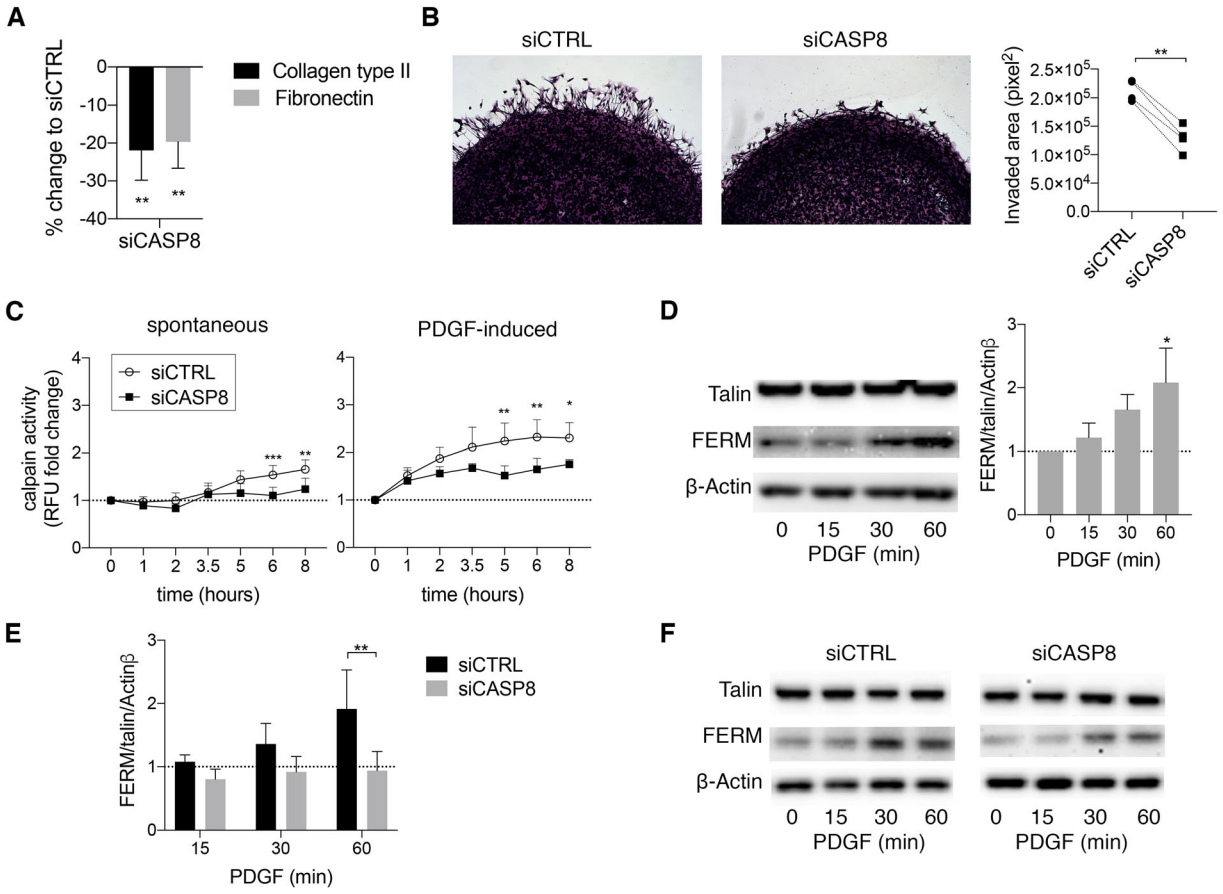


**Figure 2.** Caspase-8 takes part in FLS adhesion and invasion by modulating calpain activity and talin cleavage. (**A**) RA FLSs at 48 hours post transfection were let to adhere onto fibronectin- or collagen type II-coated plastic for 30 minutes. Graph shows mean ± SEM of the percentage of inhibition to siCTRL (n = 4). Statistical analysis was calculated comparing percentage of adhesion of siCTRL versus siCASP8; two-way ANOVA and Sidak's multiple comparison test were used. $^{**}P \leq 0.01$. (**B**) Matrigel spheroid assay was performed after 48h from FLS transfection with either siCASP8 or siCTRL. Representative 4X images of fixed and H&E stained Matrigel spheroids (left-hand side) and quantification of invaded area (right-hand side) of siCTRL and siCASP8-silenced FLSs after 24-hour PDGF. Dotted lines connect paired samples. Statistical significance was calculated with paired *t* test (n = 4). $^{**}P \leq 0.01$. (**C**) Quantification of calpain activity at different time points in RA FLSs transfected with siCASP8 or siCTRL, either spontaneous (left-hand side) or under PDGF stimulation (right-hand side). (**D**) Representative western blot showing talin, FERM domain cleavage, and actin-β in RA FLSs stimulated with 10 ng/ml PDGF for 15-30-60 minutes and densitometry quantification of FERM domain under PDGF stimulation, normalized on total talin and actin-β levels. Bars show mean ± SEM of n = 3. Paired statistical analysis was performed using Friedman test and Dunn's pos hoc test, comparing to time 0. $^{*}P \leq 0.05$. (**E**) Western blot densitometry analysis for FERM domain/talin/actin-β of siCASP8 and siCTRL RA FLSs under PDGF stimulation (0-15-30-60 min). Dotted line is baseline at time 0. Time 0 corresponded to 72 hours post transfection. (**F**) Representative western blot showing talin, FERM domain cleavage, and actin-β in RA FLSs stimulated with 10 ng/ml PDGF for 15-30-60 minutes. (**C,E**) Data were analyzed with two-way ANOVA and Sidak's multiple comparison's test. Error bars show mean ± SEM of n = 6. $^{*}P \leq 0.05$; $^{**}P \leq 0.01$; $^{***}P \leq 0.001$; $^{****}P \leq 0.0001$. FLS, fibroblast-like synoviocyte; H&E, hematoxylin and eosin; PDGF, platelet-derived growth factor; RA, rheumatoid arthritis; siRNA, small interfering RNA.

disassembly of the focal adhesion complex in cancer cells (11,14). To assess whether the catalytic activity is required in FLSs, the cells were treated with the caspase-8 inhibitor FMK-derivatized peptide Z-IETD-FMK. The inhibitor did not affect PDGF-induced FLS invasion (Figure 3A and 3C) or migration (Figure 3B and 3C).

**Tofacitinib and blocking caspase-8 have complementary effects on RA FLS pathogenicity.** To understand the effects of caspase-8 deficiency on genes related to RA, we silenced caspase-8 and performed RT-qPCR. Caspase-8 deficiency had no effect on gene expression after PDGF, tumor necrosis factor (TNF), or interleukin (IL-)1β stimulation, including matrix metalloproteinase (MMP) 1, MMP3, MMP9, IL-6, chemokine (C-C motif) ligand (CCL) 2, CCL3, chemokine (C-X-C motif) ligand (CXCL) 8, CXCL10, and granulocyte-macrophage colony-stimulating factor (GM-CSF) (Figure S2). We also determined whether combining janus kinase (JAK) inhibition using tofacitinib and caspase-8 silencing affected FLS migration. Caspase-8 significantly reduced FLS migration compared with control at all tofacitinib concentrations, indicating that the JAK/signal transducer and activator of transcription (STAT) pathway is not involved in the caspase-8-mediated effect (Figure 4A and 4B). Conversely, IL-6 and CCL2 transcript levels after PDGF or TNF stimulation were reduced by tofacitinib independent of caspase-8 silencing (Figure 4C and 4D). These data suggest that the effects of tofacitinib and caspase-8 deficiency on FLSs are independent of each other.

**RA FLS mainly express caspase-8 transcript variant G.** To determine expression and regulation of caspase-8 isoforms (A through G) in FLSs, we first evaluated our multi-omics data set. In our ChIP-seq analysis, multiple histone peaks corresponded to enhancer and promoter regions of individual caspase-8 gene

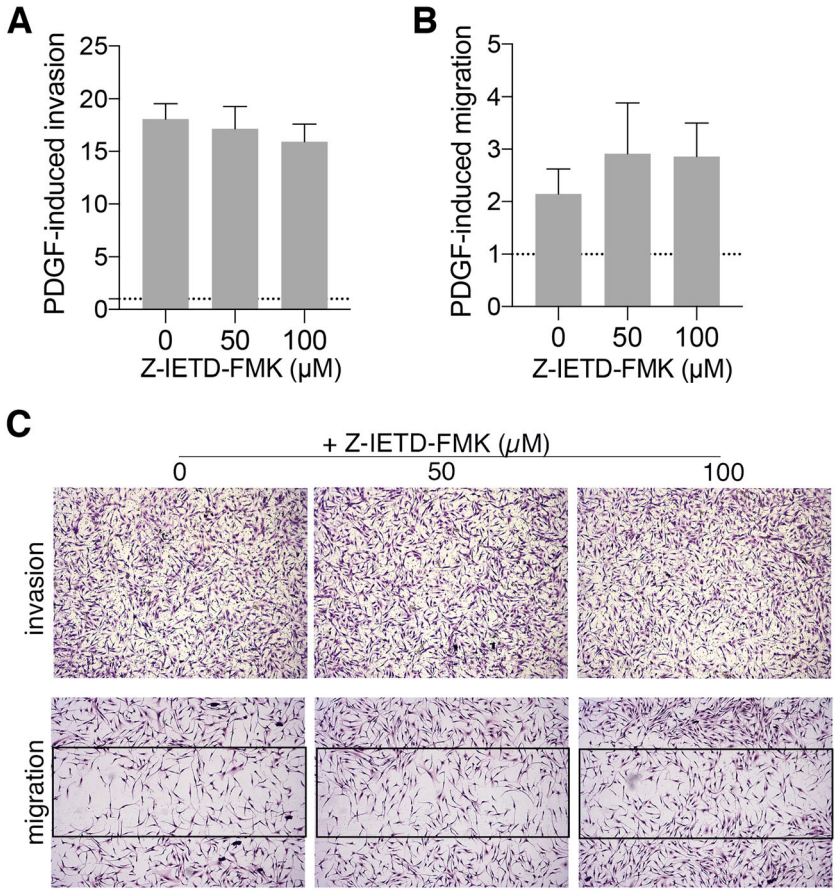


**Figure 3.** Caspase-8 involvement in cell migration and invasion is independent of caspase-8 cleavage. RA-FLSs were pre-incubated 1 hour with 50 or 100 μM Z-IETD-FMK or vehicle control (0.01% DMSO) followed by 24 hours of PDGF stimulation. (**A**) Quantification of PDGF-induced invasion and (**B**) PDGF-induced migration (calculated as fold change of %invaded area under PDGF divided %invaded area in media alone; dotted line is ctrl baseline). Media alone was used as control, and dotted line in the bar graph indicates control baseline. Error bars are mean ± SEM of n = 6 in panel A and n = 3 in panel B. (**C**) Representative 4X images of crystal violet-stained cells that had transmigrated through a Matrigel membrane (invasion assay; top) and 10X digital images of H&E staining of cells at the scratched area (migration assay; bottom) after 1 hour with 50 or 100 μM Z-IETD-FMK followed by 24 hours of PDGF stimulation. Squares indicate the scratched area. DMSO, dimethyl sulfoxide; FLS, fibroblast-like synoviocyte; H&E,hematoxylin and eosin; PDGF, platelet-derived growth factor; RA, rheumatoid arthritis.

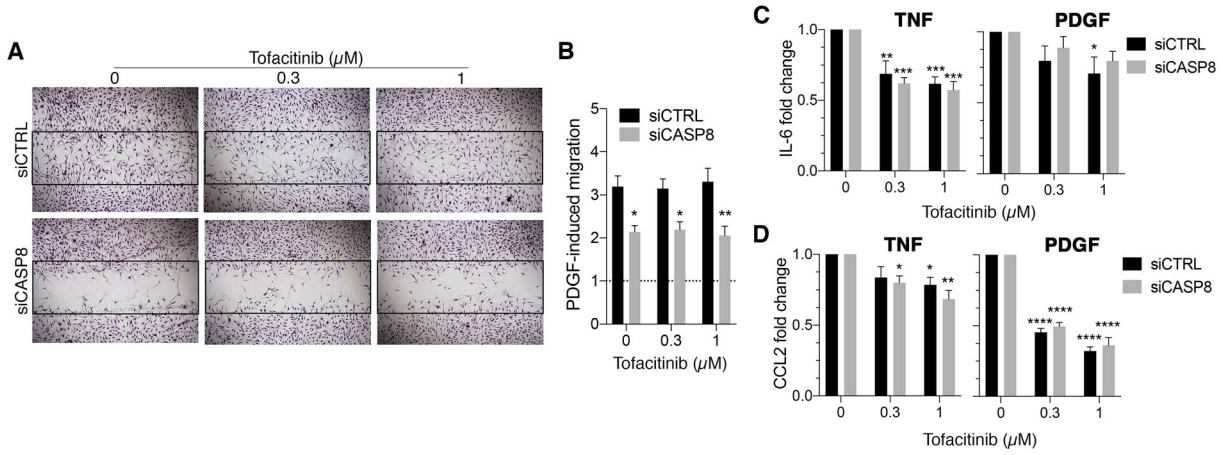


**Figure 4.** Complementary activity of tofacitinib and caspase-8 silencing on RA FLS pathogenicity. RA FLSs were transfected with siRNA targeting caspase-8 (siCASP8) or un-targeting control (siCTRL). At 48 hours post transfection, cells were stimulated for 1 hour with either vehicle control (0.01% DMSO) or 0.3-1 μM tofacitinib followed by 10 ng/ml PDGF or 50 ng/ml TNF for 24 hours. (**A**) Representative images of H&E-stained scratches of PDGF-induced migration after treatment with the inhibitor. Black lines indicate the boundaries of the scratched area used for the analysis. (**B**) Quantification of PDGF-induced migration at 24 hours (fold change on media control). Dotted line is the baseline for migration in media control. (**C**) IL-6 and (**D**) CCL2 fold change of expression (RT-qPCR, $2^{-\Delta\Delta Ct}$) at 24 hours post TNF (left-hand side graphs) or PDGF stimulation (right-hand side graphs). Data were analyzed with two-way ANOVA and Sidak's multiple comparison's test. Significancy was calculated in panel B for siCASP8 compared with siCTRL, and in panels C and D, 0.3 and 1 μM tofacitinib were compared with vehicle control (0) within each group. Error bars are mean ± SEM of n = 6. *$P \leq 0.05$; **$P \leq 0.01$; ***$P \leq 0.001$; ****$P \leq 0.0001$. CCL2, chemokine (C-C motif) ligand 2; DMSO, dimethyl sulfoxide; FLS, fibroblast-like synoviocyte; H&E, hematoxylin and eosin; IL-6, interleukin 6; PDGF, platelet-derived growth factor; RA, rheumatoid arthritis; RT-qPCR, quantitative reverse transcription PCR; siRNA, small interfering RNA; TNF, tumor necrosis factor.

isoforms (26) (Figure 5A). We noted a major peak associated with H3K4me3, four peaks for H3K27ac, and five peaks for H3K4me1 (Figure 5A-5D). The H3K4me3 mark, in particular, was similar in RA and OA FLSs and suggested that splicing variants C and G are actively transcribed (caspase-8C and -8G; Figure 5A and 5B). Of interest, nearby peaks for H3K27ac (numbers 2 and 4; Figure 5A and 5C) and one peak for H3K4me1 (number 2; Figure 5A and 5D) associated with poised transcription were significantly higher in RA than in OA FLSs (31). The histone marks correlated closely with RNA-seq data demonstrating that caspase-8C and caspase-8G are the only transcripts detected in RA FLSs, with G being substantially more abundant (Figure 5E). RT-qPCR confirmed that caspase-8G is the main variant and accounts for ~80% of total caspase-8 transcripts in RA FLSs (Figure 5F).

We then examined global expression of caspase-8 isoforms in humans using data in the Genotype-Tissue Expression (GTEx) portal (32) (https://gtexportal.org/home/gene/CASP8). Consistent with our data, we noted that caspase-8C and caspase-8G are expressed in "cultured fibroblasts," with expression also noted in certain tissues, including stomach, prostate, and pancreas. In contrast, caspase-8G expression is minimal in "transformed lymphocytes," whole blood, and tissues such as spleen, lungs, and kidneys, where -8C is the dominant variant (Figure 5G). RNA-seq analysis of RA and OA synovial tissue showed the presence of abundant transcripts for caspase-8 variants B, C, and G, indicating that CASP8G is expressed in situ (data not shown).

**Caspase-8G is induced by PDGF and regulates cell invasion and calpain activity.** We then evaluated the regulation of caspase-8C and -8G expression in RA FLSs and found that only caspase-8G was induced by PDGF and reduced by IL-1β whereas TNF had no effect (Figure 6A). We also observed that caspase-8G was increased during active cell growth and further enhanced by PDGF (Figure 6B). No differences between RA and OA FLSs were found in PDGF-induced caspase-8G expression (Figure S3).

Caspase-8G was initially described in the context of cell apoptosis in cancer cells (33). However, we did not see evidence of cell death nor detect cleaved caspase-8 by western blot analysis. To further investigate the function of caspase-8G in RA FLSs, we silenced either total caspase-8 or only caspase-8G and found that caspase-8G alone accounts for regulation of PDGF-induced migration and calpain activity (Figure 6C and 6D). We also evaluated the expression of caspase-8 isoforms in a transformed fibroblast line, namely HS68 cells. Those cells also express mainly caspase-8G and silencing caspase-8 significantly reduced PDGF-induced invasion by ~50% (Figure S4). Therefore caspase-8G, and not C, is implicated in tumor as well as FLS invasion. Our epigenetic data indicate that FLSs have epigenetic marks that could favor caspase-8G transcription due to poised regulatory

regions and might lead to increased expression in the context of chronic inflammation.

**Structure and evolution of the caspase-8G variant.** To explore the structure of caspase-8G, we aligned NCBI RefSeq (26) of all predicted and characterized splicing transcripts of caspase-8 and found that caspase-8G contains a unique 59 amino acid N-terminal sequence. Variant B is identical to G but lacks the N-terminal domain (Figure S5). No functional or structural domains were found in the extended N-terminal region, and a secondary structure was not predicted to form in this region (Figure 6E). Caspase-8B and -8G DED domains were cloned into *Escherichia coli* and purified for crystal structure determination. The 59 amino acid N-terminal sequence of isoform G was not visible, indicating a lack of stable interactions with the DED domain (Figure S6). Aside from the disordered N-terminal tail of caspase-8G, the crystal structure showed nearly perfect alignment of the caspase-8 DED domains of variants B and G (Figure 6F).

The caspase-8G splicing variant is found only among primates (Figure 6G). In particular, the Hominidae family have the full-length G-specific domain, with the Chimpanzee (*Pan*

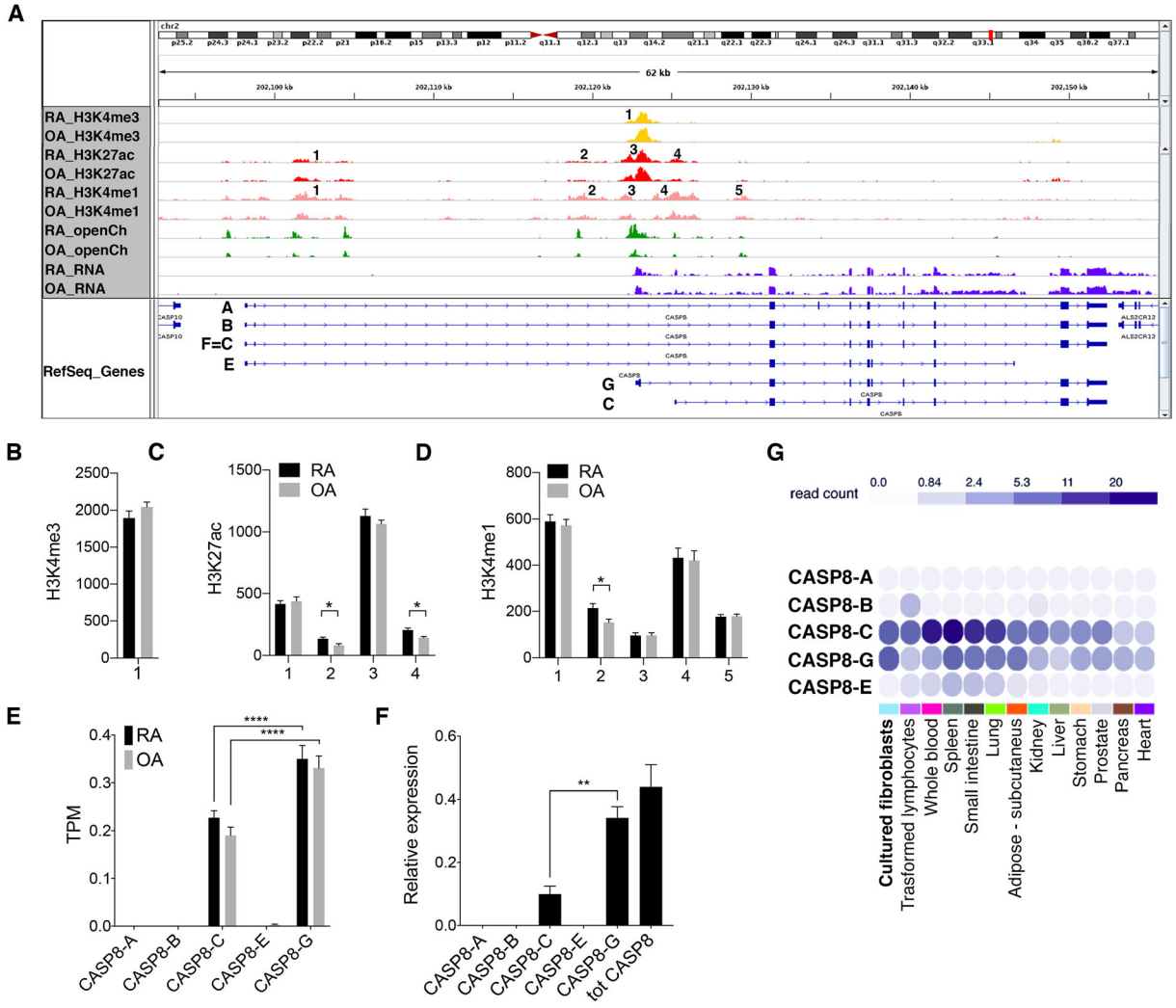


**Figure 5.** RA FLSs mainly express caspase-8 variant G. (**A**) Epigenomic landscape of *CASP8* gene, with three histone modifications, open chromatin, and RNA-seq, and transcript-coding variants (Refseq database) (26). The figure is an example of the relative signal intensity across a selected region of the genome for each mark in RA and OA FLSs. In addition, the locations across chromosomes for the selected regions are indicated, peaks analyzed are numbered, and Refseq transcripts annotated. (**B-D**) Quantification of H3K4me3, H3K4me1, and H3K27ac peak intensity and (**E**) RNAseq analysis, in RA and OA FLSs (n = 10-11). *P* values were calculated with two-way ANOVA and Sidak's post hoc test. **P* ≤ 0.05; ***P* ≤ 0.01. (**F**) Relative expression of caspase-8 variants determined by RT-qPCR (n = 6). (**B-F**) Error bars show mean ± SEM. Two-way ANOVA and Sidak's post hoc test were used for the statistical analysis. **P* ≤ 0.05; ***P* ≤ 0.01; ****P* ≤ 0.001; *****P* ≤ 0.0001. (**G**) Caspase-8 isoform expression in selected tissue compartments, obtained from the Genotype-Tissue Expression (GTEx) portal. For visual purposes, the image was rearranged and adapted from the original downloaded at https://gtexportal.org/home/gene/CASP8. FLS, fibroblast-like synoviocyte; OA, osteoarthritis; RA, rheumatoid arthritis; RNAseq, RNA sequencing; RT-qPCR, quantitative reverse transcription PCR.

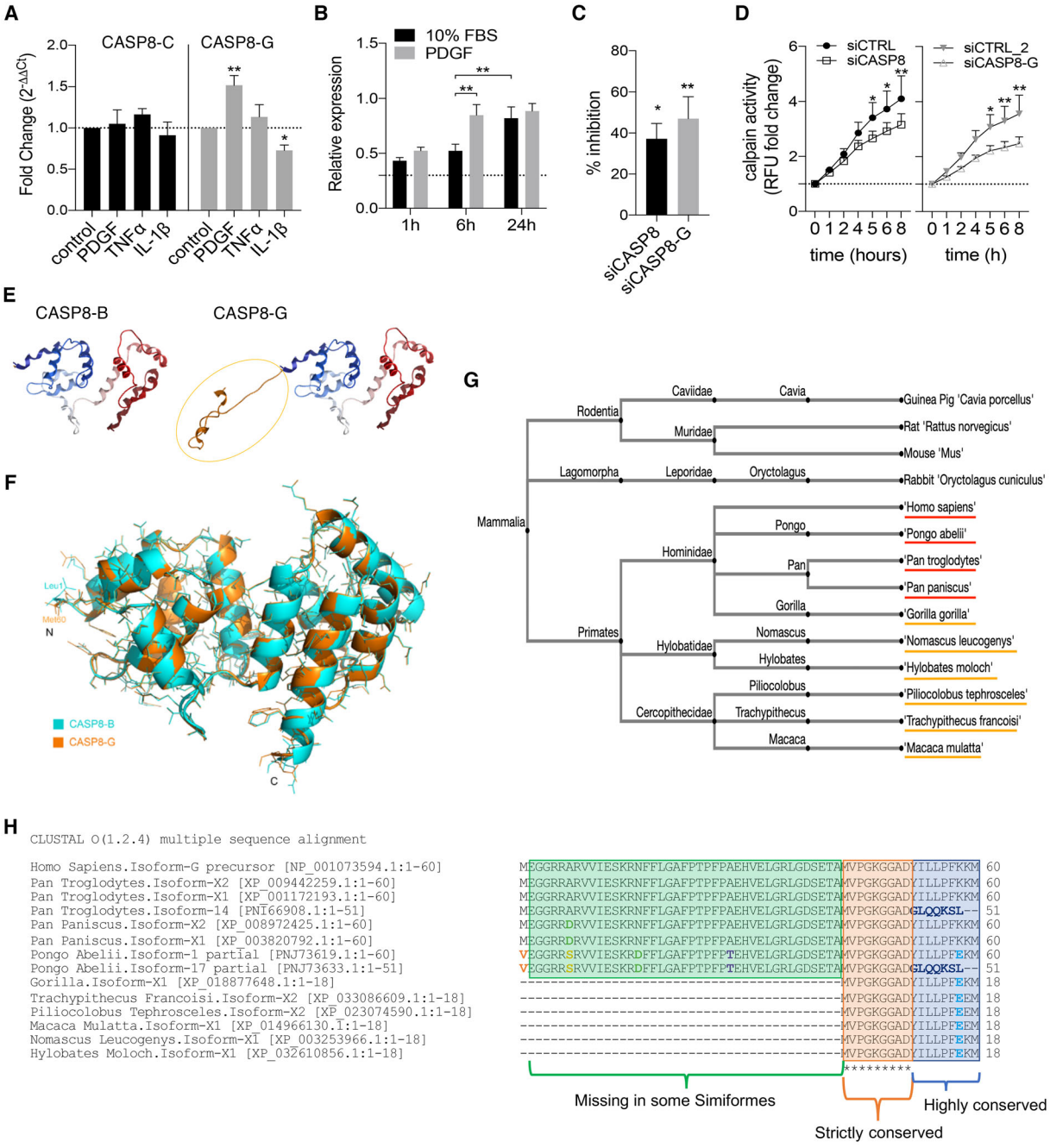


**Figure 6.** PDGF induces caspase-8G, which in turn regulates invasion and calpain activity and is characterized by a unique N-term domain. (**A**) Caspase-8C (CASP8-C) and -8G (CASP8-G) mRNA expression after 6 hours of PDGF (10 ng/ml), TNF (50 ng/ml), or IL-1β (2 ng/ml) stimulation; fold changes to 10% FBS controls (n = 6). (**B**) PDGF time course (1, 6, and 24 h) for CASP8-G mRNA expression in RA FLSs (n = 3). (**A,B**) Error bars show mean ± SEM. Statistical significance was calculated with two-way ANOVA and Sidak's post hoc test, comparing all data to controls. $^{*}P \le 0.05$; $^{**}P \le 0.01$. (**C,D**) RA FLSs were transfected with siRNA either targeting total caspase-8 (siCASP8) or targeting caspase-8G only (siCASP8-G) and respective scramble controls (siCTRL and siCTRL-2). (**C**) Transmigrated FLSs through a Matrigel membrane after 24 hours of PDGF stimulation were stained with Crystal violet, and percentage of inhibition of PDGF-induced invasion (mean ± SEM) was calculated from PDGF fold changes over media alone of siCASP8 and siCASP8-G compared with respective siCTRLs. Statistical significance assessed with Wilcoxon matched-pairs signed rank test comparing PDGF-induced fold changes of siCASP8/siCTRL or of siCASP8-G/siCTRL-2 (n = 6). $^{*}P \le 0.05$; $^{**}P \le 0.01$. (**D**) Quantification of calpain activity under PDGF stimulation (0-8 h) in samples transfected with siCASP8 (left) or siCASP8-G (right) and respective controls. Data were analyzed with two-way ANOVA and Sidak's multiple comparison's test. Error bars show mean ± SEM of n = 6. $^{*}P \le 0.05$; $^{**}P \le 0.01$; $^{***}P \le 0.001$. (**E**) Predicted protein structure of caspase-8 variant B (CASP8-B) and G (CASP8-G) DED domain; unique unstructured N-term domain of CASP8-G is circled in yellow. (**F**) Structural superposition of the DED domain structures of CASP8 isoforms B (cyan) and G (orange), shown as a ribbon diagram with all sidechains represented as wireframes. The root-mean-square deviation (RMSD) is

*(Figure legend continues on next page.)*

*troglodyte*) having 100% homology. Only a few other species belonging to the Hylobatidae and Cercopithecidae family display a partial domain (Figure 5G and 5H). Animals of the Hylobatidae family diverged from the common ancestor about 16.8 million years ago and represent a bridge between "old-world" primates (which includes the Cercopithecidae family) and "new-world" great apes (the Hominidae family) (34). Therefore, caspase-8G might have been a positive selected gene during great ape evolution.

## DISCUSSION

RA is a complex immune-mediated disorder characterized by synovial hyperplasia and infiltration with innate and adaptive immune cells (1). FLSs participate in RA pathogenesis, particularly as mediators of joint damage through enhanced invasiveness and elaboration of cytokines and proteases (2,5). RA FLSs exhibit these behaviors in part through their response to environmental stimuli, although their aggressive phenotype also results from epigenetic imprinting (4–6). Alterations in cell cycle, cell adhesion, and extracellular matrix pathways are consistently abnormal in RA.

Comprehensive epigenetic landscape analysis that integrated the transcriptome, DNA methylome, chromatin accessibility, and histone marks highlights differences between RA and non-RA FLSs. The data implicated unexpected mechanisms that could contribute to RA, such as the Huntington disease pathway; at least one molecule in that pathway, HIP-1, has been biologically validated (6). In reviewing our epigenetic databases, *CASP8* also emerged as a gene of interest (6,8). In addition to abnormal marks in *CASP8*, indirect evidence also suggested its relevance because the gene is downstream of HIP-1 in the Huntington disease pathway. Therefore, we focused our attention on understanding the function and regulation of caspase-8 in FLSs.

Several studies have evaluated caspase-8 enzymatic activity and its association with apoptosis (35). In contrast, recent evidence indicates that caspase-8 can regulate cell adhesion and motility in malignant cells independent of its enzymatic pro-apoptotic function (9,10). In cancer cell lines, caspase-8 pro-enzyme localizes at the focal adhesions and can promote metastasis growth and cell migration and adhesion (11). The catalytic domain, but not the catalytic activity, is required for caspase-8-dependent regulation of calpain and cell adhesion (9,14). In our study, caspase-8 also played a key role in primary non-tumor cells, namely FLSs, and their adhesion to extracellular matrix proteins as well as PDGF-induced migration and invasion independent of catalytic activity.

One key finding was the identification of variant G as the primary isoform expressed in FLSs. The G variant was induced by PDGF and is responsible for caspase-8 function on PDGF-induced calpain activity and the effect on invasion. Caspase-8G is unique among the isoforms because it is characterized by a 59 amino acid sequence at the N-terminus of the first DED domain of the pro-caspase. Although the catalytic domain of caspase-8 is sufficient for its effect at the focal adhesions, DEDs of caspase-8 alone recreate the adhesive and biochemical phenotypes observed with the full-length protein (36). This phenomenon is associated with caspase-8 localization at the leading edge of cellular lamellae and its ability of influencing growth factor signaling via its association with proto-oncogene tyrosine-protein kinase Src (37). This highlights the importance of the DED domain in directing caspase-8 localization and suggests a possible role for the N-terminal sequence of caspase-8G.

More detailed evaluation of caspase-8G structure showed that the unique N-terminus tail is disordered and likely lacks stable interactions with the DED domain. This creates challenges for selectively targeting the G splice variant with a small molecule inhibitor. Alternatively, the tail could potentially interact with other proteins that are responsible for the unique biology of caspase-8G. The fact that this variant is a relatively recent evolutionary advance also limits the utility of preclinical studies that explore the biology. Possible approaches for biologic validation of this target *in vivo* might require transgenic animals expressing either caspase-8B or -G.

The biology of caspase-8G creates opportunities to target FLS invasiveness selectively without immunosuppression. For instance, inhibiting JAK/STAT pathways is a validated therapeutic approach in RA that inhibits cytokine signaling and blocks FLS inflammatory responses (38–40). Tofacitinib, like other JAK inhibitors, is only effective in a subset of RA patients (39,41,42). Because JAK/STAT and caspase-8 functions do not overlap, combining these approaches might be effective in RA without additive effects on host defense encountered in other combinations (43). This approach could leverage the nonenzymatic functions of caspase-8G by selectively targeting this isoform independent of its enzymatic functions associated with apoptosis

*(Figure legend continued from previous page.)*
0.206 Å. The N-terminus is labeled with the first visible residues Leu1 (isoform B) and Met60 (isoform G). The figure was generated with PyMOL. (**G**) Phylogenetic tree for CASP8-G. Species with full length N-term domain are underlined in red and those with partial domain in yellow. (**H**) Alignment analysis of the first 60 amino acids of the N-term domain of caspase-8G with homolog sequences in primates. Highlights are the conserved area among different species. Stars mark strictly conserved area. DED, dead-effector domain; FBS, Fetal bovine serum; FLS, fibroblast-like synoviocyte; IL-1β, interleukin 1β; PDGF, PDGF, platelet-derived growth factor; RA, rheumatoid arthritis; siRNA, small interfering RNA; TNF, tumor necriosis factor.

and immune responses. The unique N-term tail of variant G offers a unique opportunity for targeting this isoform, but it will likely require allosteric inhibitors or blocking the activity of interacting molecules due to the lack of structure.

Defining the role of caspase-8G and its interacting partners could be an important next step in defining the biology of this splice variant. These studies also demonstrate how integrative analysis of multiple omics data sets can reveal nonobvious pathways. Prioritizing the rich landscape of genes identified by these methods could provide insight into the imprinted aggressive phenotype of RA FLS or cells from other immunologic diseases.

## ACKNOWLEDGMENTS

The authors thank Amanda Kuhs and Wenru Yu for helping with tissue culture and sample processing and Marc E. Rutter, Milan Maletic, and Marijane Russell for cloning and protein expression. They acknowledge the European Synchrotron Radiation Facility (ESRF) for providing access to synchrotron radiation facilities, and they thank Romain Talon for assistance in using beamline ID30B (for caspase-8 isoform G data).

This research used resources of the Advanced Photon Source, a U.S. Department of Energy (DOE) Office of Science User Facility, operated for the DOE Office of Science by Argonne National Laboratory under Contract DE-AC02-06CH11357. Use of the Lilly Research Laboratories Collaborative Access Team (LRL-CAT) beamline at Sector 31 of the Advanced Photon Source was provided by Eli Lilly Company, which operates the facility.

## AUTHOR CONTRIBUTIONS

All authors were involved in drafting the article or revising it critically for important intellectual content, and all authors approved the final version to be published.

**Study conception and design.** Ansalone, Nygaard, Hammaker, Mertsching, Benschop, Boyle, Wang, Firestein.

**Acquisition of data.** Ansalone, Weichert, Tung, Kodapani, Sauder.

**Analysis of data.** Ansalone, Ainsworth, Nygaard, Ai, Prideaux, Hammaker, Weichert, Tung, Kodapani, Sauder, Perumal, Wang, Mertsching, Benschop, Boyle, Firestein.

## REFERENCES

1. Smolen JS, Aletaha D, Barton A, Burmester GR, Emery P, Firestein GS, et al. Rheumatoid arthritis. Nat Rev Dis Prim 2018;4:1–23.
2. Bartok B, Firestein GS. Fibroblast-like synoviocytes: key effector cells in rheumatoid arthritis. Immunol Rev 2010;233:233–55.
3. Choy EH, Kavanaugh AF, Jones SA. The problem of choice: current biologic agents and future prospects in RA. Nat Rev Rheumatol 2013;9:154–63.
4. Nygaard G, Firestein GS. Restoring synovial homeostasis in rheumatoid arthritis by targeting fibroblast-like synoviocytes. Nat Rev Rheumatol 2020;16:316–33.
5. Bottini N, Firestein GS. Duality of fibroblast-like synoviocytes in RA: passive responders and imprinted aggressors. Nat Rev Rheumatol 2013;9:24–33.
6. Ai R, Laragione T, Hammaker D, Boyle DL, Wildberg A, Maeshima K, et al. Comprehensive epigenetic landscape of rheumatoid arthritis fibroblast-like synoviocytes. Nat Commun 2018;9:1921.
7. Laragione T, Brenner M, Lahiri A, Gao E, Harris C, Gulko PS. Huntingtin-interacting protein 1 (HIP1) regulates arthritis severity and synovial fibroblast invasiveness by altering PDGFR and Rac1 signalling. Ann Rheum Dis 2018;77:1627–35.
8. Whitaker JW, Boyle DL, Bartok B, Ball ST, Gay S, Wang W, et al. Integrative omics analysis of rheumatoid arthritis identifies non-obvious therapeutic targets. PLoS One 2015;10:e0124254.
9. Graf RPP, Keller N, Barbero S, Stupack D. Caspase-8 as a regulator of tumor cell motility. Curr Mol Med 2014;14:246–54.
10. Keller N, Ozmadenci D, Ichim G, Stupack D. Caspase-8 function, and phosphorylation, in cell migration. Semin Cell Dev Biol 2018;82:105–17.
11. Barbero S, Mielgo A, Torres V, Teitz T, Shields DJ, Mikolon D, et al. Caspase-8 association with the focal adhesion complex promotes tumor cell migration and metastasis. Cancer Res 2009;69:3755–63.
12. Helfer B, Boswell BC, Finlay D, Cipres A, Vuori K, Tae BK, et al. Caspase-8 promotes cell motility and calpain activity under nonapoptotic conditions. Cancer Res 2006;66:4273–8.
13. Huttenlocher A, Horwitz AR. Integrins in cell migration. Cold Spring Harb Perspect Biol 2011;3:a005074.
14. Barbero S, Barilà D, Mielgo A, Stagni V, Clair K, Stupack D. Identification of a critical tyrosine residue in caspase 8 that promotes cell migration. J Biol Chem 2008;283:13031–14.
15. Arnett FC, Edworthy SM, Bloch DA, Mcshane DJ, Fries JF, Cooper NS, et al. The American Rheumatism Association 1987 revised criteria for the classification of rheumatoid arthritis. Arthritis Rheum 1988;31:315–24.
16. Aketata D, Neogi T, Silman A, Funovits J, Felson D, Bingham C, et al. Rheumatoid arthritis classification criteria: an American College of Rheumatology/European League Against Rheumatism collaborative initiative. Arthritis Rheumatol 2010;62:2569–81.
17. Bartok B, Boyle DL, Liu Y, Ren P, Ball ST, Bugbee WD, et al. PI3 kinase δ is a key regulator of synoviocyte function in rheumatoid arthritis. Am J Pathol 2012;180:1906–16.
18. Rosengren S, Boyle DL, Firestein GS. Acquisition, culture, and phenotyping of synovial fibroblasts. Methods Mol Med 2007;135:365–75.
19. Schmittgen TD, Livak KJ. Analyzing real-time PCR data by the comparative CT method. Nat Protoc 2008;3:1101–8.
20. Nygaard G, Paolo JA Di, Hammaker D, Boyle DL, Budas G, Notte GT, et al. Regulation and function of apoptosis signal-regulating kinase 1 in rheumatoid arthritis. Biochem Pharmacol 2018;151:282–90.
21. Bartok B, Hammaker D, Firestein GS. Phosphoinositide 3-kinase δ regulates migration and invasion of synoviocytes in rheumatoid arthritis. J Immunol 2014;192:2063–70.
22. Dobin A, Davis CA, Schlesinger F, Drenkow J, Zaleski C, Jha S, et al. STAR: Ultrafast universal RNA-seq aligner. Bioinformatics 2013;29:15–21.
23. Li B, Dewey CN. RSEM: accurate transcript quantification from RNA-Seq data with or without a reference genome. BMC Bioinformatics 2011;12:323.
24. Kent WJ, Sugnet CW, Furey TS, Roskin KM, Pringle TH, Zahler AM, et al. The Human Genome Browser at UCSC. Genome Res 2002;12:996–1006.
25. Lander ES, Linton LM, Birren B, Nusbaum C, Zody MC, Baldwin J, et al. Initial sequencing and analysis of the human genome. Nature 2001;409:860–921.
26. O'Leary NA, Wright MW, Brister JR, Ciufo S, Haddad D, McVeigh R, et al. Reference sequence (RefSeq) database at NCBI: current status, taxonomic expansion, and functional annotation. Nucleic Acids Res 2016;44:D733–45.

27. Madeira F, Park Y mi, Lee J, Buso N, Gur T, Madhusoodanan N, et al. The EMBL-EBI search and sequence analysis tools APIs in 2019. Nucleic Acids Res 2019;47:W636–41.
28. Federhen S. The NCBI taxonomy database. Nucleic Acids Res 2012; 40:D136–43.
29. Robinson O, Dylus D, Dessimoz C. Phylo.io: interactive viewing and comparison of large phylogenetic trees on the web. Mol Biol Evol 2016;33:2163–6.
30. Franco SJ, Huttenlocher A. Regulating cell migration: calpains make the cut. J Cell Sci 2005;118:3829–38.
31. Dong X, Weng Z. The correlation between histone modifications and gene expression. Epigenomics 2013;5:113–6.
32. Lonsdale J, Thomas J, Salvatore M, Phillips R, Lo E, Shad S, et al. The Genotype-Tissue Expression (GTEx) project. Nat Genet 2013;45: 580–5.
33. Breckenridge DG, Nguyen M, Kuppig S, Reth M, Shore GC. The procaspase-8 isoform, procaspase-8L, recruited to the BAP31 complex at the endoplasmic reticulum. Proc Natl Acad Sci 2002;99: 4331–6.
34. Steiper ME, Young NM, Sukarna TY. Genomic data support the hominoid slowdown and an Early Oligocene estimate for the hominoid-cercopithecoid divergence. Proc Natl Acad Sci U S A 2004;101: 17021–6.
35. Williams B, Dharmapatni A, Crotti T. Intracellular apoptotic pathways: a potential target for reducing joint damage in rheumatoid arthritis. Inflamm Res 2018;67:219–31.
36. Finlay D, Vuori K. Novel noncatalytic role for caspase-8 in promoting Src-mediated adhesion and Erk signaling in neuroblastoma cells. Cancer Res 2007;67:11704–11.
37. Finlay D, Howes A, Vuori K. Critical role for caspase-8 in epidermal growth factor signaling. Cancer Res 2009;69:5023–9.
38. Rosengren S, Corr M, Firestein GS, Boyle DL. The JAK inhibitor CP-690,550 (tofacitinib) inhibits TNF-induced chemokine expression in fibroblast-like synoviocytes: autocrine role of type I interferon. Ann Rheum Dis 2012;71:440–7.
39. Boyle DL, Soma K, Hodge J, Kavanaugh A, Mandel D, Mease P, et al. The JAK inhibitor tofacitinib suppresses synovial JAK1-STAT signalling in rheumatoid arthritis. Ann Rheum Dis 2014;74:1311–6.
40. Hammaker D, Nygaard G, Kuhs A, Ai R, Boyle DL, Wang W, et al. Joint location–specific JAK-STAT signaling in rheumatoid arthritis fibroblast-like synoviocytes. ACR Open Rheumatol 2019;1:640–8.
41. Hodge JA, Kawabata TT, Krishnaswami S, Clark JD, Telliez JB, Dowty ME, et al. The mechanism of action of tofacitinib—an oral Janus kinase inhibitor for the treatment of rheumatoid arthritis. Clin Exp Rheumatol 2016;34:318–28.
42. Dhillon S. Tofacitinib: a review in rheumatoid arthritis. Drugs 2017;77: 1987–2001.
43. Genovese MC, Cohen S, Moreland L, Lium D, Robbins S, Newmark R, et al. Combination therapy with etanercept and anakinra in the treatment of patients with rheumatoid arthritis who have been treated unsuccessfully with methotrexate. Arthritis Rheum 2004;50: 1412–9.